

OBTAINING HYDRAULIC PROPERTIES OF UNCONSOLIDATED POROUS MATERIAL

Michael L. Turner^{1,2}, Christoph H. Arns¹, Arthur Sakellariou¹, Tim J. Senden¹, Adrian P. Sheppard¹, Robert M. Sok¹, Ajay Limaye³ & Mark A. Knackstedt¹

¹Department of Applied Mathematics, Research School of Physical Sciences and Engineering, Australian National University, ACT, 0200

²CRC LEME, Department of Earth and Marine Sciences, Australian National University, ACT, 0200

³VizLab, ANU Supercomputing Facility, ACT 0200, Australia

INTRODUCTION

In order to gain a precise knowledge of hydraulic properties characterising unconsolidated regolith material an accurate description of the physical characteristics at the pore-scale is necessary (Solymar & Fabricius 1999, Lin & Miller 2004). Unfortunately this is generally unavailable (Sahimi 1993, Ruan & Illangasekare 1999, Pan *et al.* 2004). At the pore-scale the influence the matrix imposes on contaminant migration, gas nucleation and mixed liquid phases can be included in a description of the entire sample (Vogel & Roth 1998, Solymar & Fabricius 1999, Pan *et al.* 2004). X-ray tomography can reliably describe the pore structure and connectivity of real samples (Turner *et al.* 2003). Thus, hydraulic properties can be extracted from simulations at the pore scale.

ACQUIRING THE SAMPLE

The micro X-ray tomographic technique has been described in detail for consolidated samples (Knackstedt *et al.* 2004). However, the major hurdle in gaining precise knowledge of the hydraulic properties of an unconsolidated sample is to acquire the sample without disturbing the natural structure. A large part of this investigation involved overcoming this difficulty. The samples used in this study were acquired in the field from the 50.55-50.85 m interval using the PQ coring technique (The Australian Drilling Industry Training Committee Ltd. 1997). This method involves a hollow barrel nominally 90 mm inside diameter with a diamond bit on the cutting face. The diamond cutting bit is a ring that is slowly driven into the ground as it rotates, cutting a cylindrical section of material which slides up into the hollow barrel as the barrel moves down into the surrounding material removing the material from the ground with a minimum of disturbance.

SUBSAMPLING OF THE MATERIAL FOR IMAGING AT THE MICRO-SCALE.

After the core material was recovered, it was stored and transported in a sealed 90 mm diameter PVC tube and kept at 4°C until it was removed for subsampling. Subsampling the original core sample was achieved using a simple purpose built apparatus to remove a cylindrical section 35mm long and 16mm in diameter (Figure 1).

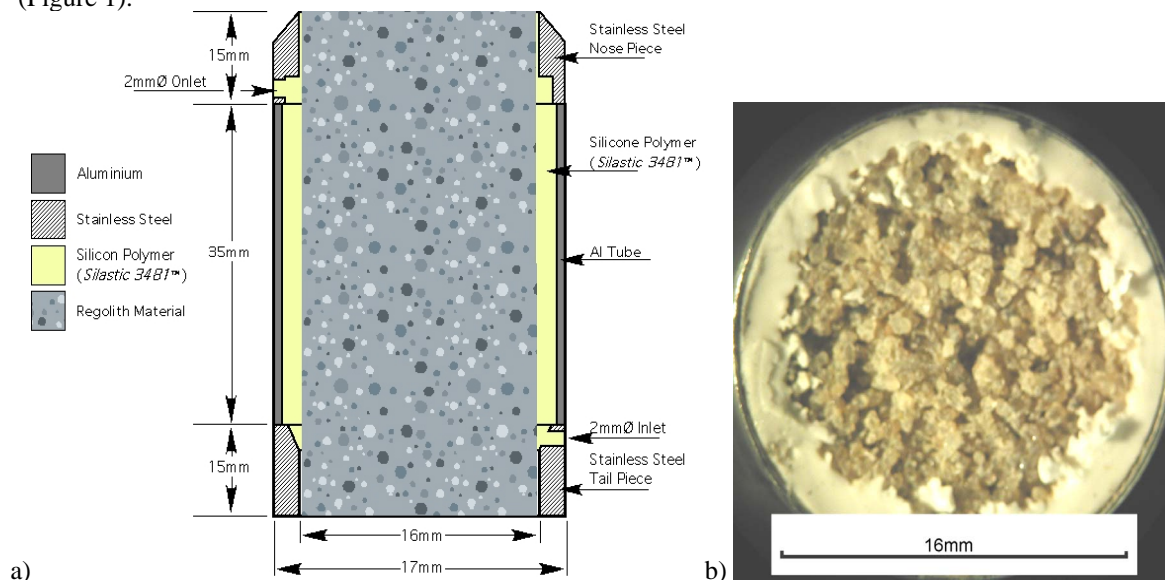
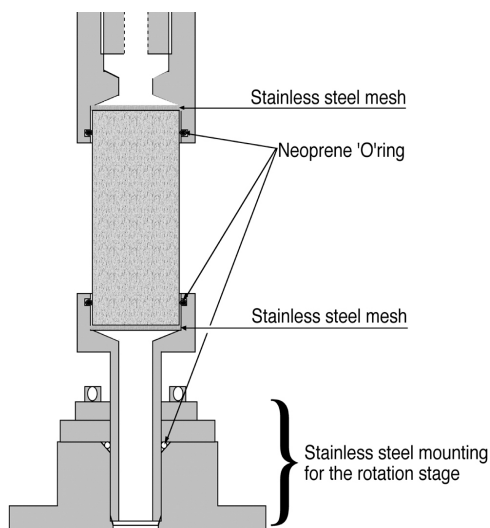


Figure 1: a) Schematic of the subsampling device after the subsample was taken and injection of silicon. Horizontal exaggeration 2:1. b) Plan view of the Al chamber after removal of the nose and tail pieces. c) (next page) Sample mounted on the rotation stage of the X-ray CT.



The subsampling device was designed to leave a 1 mm void between the inner wall of the Al chamber and the sample. A silicone mould-making polymer was injected at a rate of approximately 2 ml/hr from the bottom into the space through the 2 mm inlet to fill the space between the chamber walls and the sample, thereby removing any artificial flow paths, and providing a known no-flow boundary (Figure 1a and b). The polymer invaded the sample to a depth of up to 2 grains thereby removing any zone of disturbance due to the subsampling process as noted by Burger & Belitz (1997). The 2 mm outlet in the nose piece is for overflow of the polymer once the void space had been filled. The nose and tail pieces are then carefully removed. The Al chamber is then fitted to a purpose built adapter that allows the sample to be mounted on the rotation stage of the X-ray CT (Figure 1c)

DETERMINING THE PHYSICAL AND HYDRAULIC PROPERTIES

Particle Sizing

Particle sizing was performed by a Saturn DigiSizer 5200 laser sizer operated at Particle & Surface Sciences Pty. Limited, Gosford Australia (Particle and Surface Sciences Pty. Ltd. 2004). This machine is a static light scattering particle size analyzer and results are given as volume frequency percent. Data reduction is accomplished by reproducing the experimental data set from Mie theory calculations (see Jones 2003). Discussion on this process can be found in Loizeau *et al.* (1994).

Grain-size was also obtained using the sieve-hydrometer method. This method involves measurement of the silt and clay, or suspended fraction, by recording the displacement volume of a hydrometer suspended in the solution and then the physical sieving of the granular component to obtain a weight percent fraction (See American Society for Testing and Materials 1990). Sand, silt and clay are defined according to the Australian texture diagram (Marshall 1947) where clay is $< 2 \mu\text{m}$, silt is $2\text{--}20 \mu\text{m}$ and sand $20\text{--}2000 \mu\text{m}$. Using this classification scheme and using both the laser sizing and sieve-hydrometer results this material could be classified as either a loamy sand or sandy loam, respectively.

MICRO FOCUS X-RAY COMPUTED TOMOGRAPHY (X-RAY CT)

The data obtained from this process reflects the relative density of each volume element (voxel) of the sample and can easily distinguish the difference between water, air and solid. The X-ray CT consists of a micro-focus X-ray source (X-Tek), a high resolution X-ray camera (Roper, PI-SCX100: 2048) and a rotation stage (RV120PP, Newport). The X-ray source is capable of energies in the range of 30–225 kV, the X-ray camera is capable of radiographs with a size of 2048×2048 pixels and the rotation stage is capable of 0.1 degree steps. To non-destructively image the internal structure a series of radiographs are collected by rotating the sample through 360 degrees. These radiographs are then reconstructed with custom made software based on the Feldkamp technique (Feldkamp *et al.* 1984) to generate a tomogram dataset of the sample. Since the X-ray CT has a cone beam geometry, the spatial resolution of the tomogram can be set by simply adjusting the distance between the X-ray source and the sample and the distance between the X-ray source and the X-ray camera. A detailed synopsis of the process can be found in Sakellariou *et al.* (2004).

For this experiment, the sample was analysed with the X-ray source set at an acceleration voltage of 80 kV and a current of $200 \mu\text{A}$, using a 3 mm silica filter to reduce beam hardening artifacts and a cone beam angle of 2° . Some 3000 projections were collected, each projection was 2048^2 pixels and it took 32 hours to collect the data. The resulting volume dataset was 2048^3 voxels with a voxel size $9.4 \mu\text{m}$ and was 32 GB in size.

DATA OBTAINED

Figure 2 shows a single plane through the reconstructed 3-D dataset. The figures from left to right are the complete dataset, (false colour), void only, granular material only, particulates below the voxel size of this image ($9.4 \mu\text{m}$) and the 3 partitions overlaid on one another respectively. From this partitioning of the 3D dataset or segmentation, grain size distribution, grain shape, pore size distribution, porosity, and permeability data are obtainable.

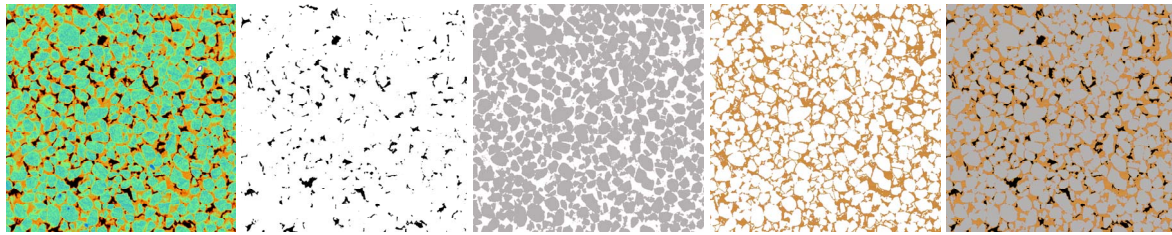


Figure 2: From left to right: the original dataset; voids only, shown as black; granular material only; material below the voxel size/resolution of this image ($9.4\ \mu\text{m}$), defined as silt/clay; and, the 3 partitions overlaid on one another. Each image is the same region of the same slice and contains $28\ \text{mm}^2$. The voxel/pixel size of the data is $9.4\ \mu\text{m}$.

The same data can also be visualised in 3D (Figure 3).

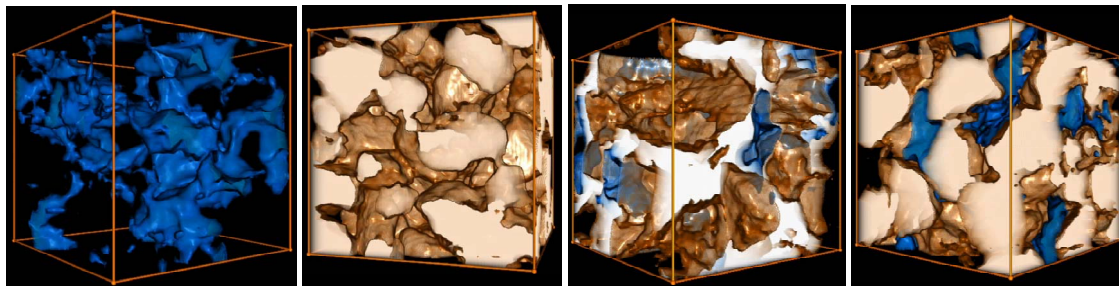


Figure 3: From left to right: void phase only (blue); grain phase only (white); clay (white) and void (blue) grains are transparent and the grain surfaces are brown; and, grain (white) and void (blue) with clay removed. These images represent a subvolume (64^3) of the total dataset.

From the data obtained using the imaging technology coupled with a method of subsampling that does not disturb the natural geometry of the material, parameters that are routinely estimated using pedotransfer functions such as pore-size distribution, porosity and permeability (Wösten *et al.* 2001, Fredlund *et al.* 2002) can now be obtained directly.

From a cursory examination of the images in Figure 3 it can be seen that parameters such as grain shape and size, connectivity and size of the pore space, phase morphology or distribution, interface surface area and other physical properties are readily available. It can be seen for example that the clay phase is pore filling in contrast to pore lining; this has obvious importance when pore connectivity and permeability are crucial parameters as they often are.

PHYSICAL PROPERTIES

The grain-size distribution and shape characterisation, including roundness and sphericity, are often measured descriptors for granular material. Shape description can be a subjective parameter that is usually measured by visual comparison of grains with a set of standard images (see Powers 1953). From the 3D images generated using the technique presented here, grain shape can be examined by fitting predetermined shapes into the discretized phase labelled grain. Grain-size is calculated by two methods: a) by growing spheres into the phase delineated as grain until the growth is confined by the grain boundaries; and, b) by calculating the chord length along the grain phase for each of the three directions. The same process is performed on the other phases. Other algorithms to ascertain these parameters are undergoing development. Preliminary results including comparing the results obtained here with those obtained traditionally are encouraging (Figure 4).

COMPARISON WITH OTHER METHODS

Mean grain-size measured by laser diffraction was $398.3\ \mu\text{m}$. As the laser sizing technique reported no grains in the $126\text{--}38\ \mu\text{m}$ range showing a clear bi-modal distribution, mean grain-size of only the coarse fraction ($> 38\ \mu\text{m}$ fraction) was used to compare to the image data as this technique lumped all material below resolution into the clay/silt phase. This recalculated mean was $426\ \mu\text{m}$ compared to the mean calculated from chord length, $448\ \mu\text{m}$, and inscribed spheres $263\ \mu\text{m}$. Sieve-hydrometer measurements reported no material in the $2\text{--}175\ \mu\text{m}$ range, maybe reflecting the less comprehensive nature of the dataset.

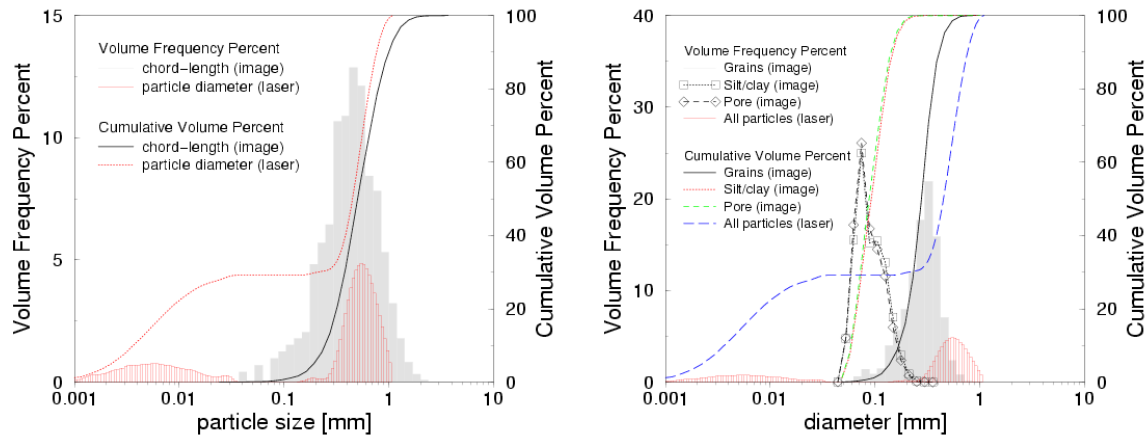


Figure 4: Left hand graph - particle-size determined by chord length and laser sizing. **Right hand graph** - pore-size distribution, particle-size and the size of the bulk clay/silt domains as measured by maximal inscribed spheres, and particle-size determined by laser sizing. Size data measured in the image analysis has a lower bound governed by image resolution and all material not resolvable is labelled silt/clay.

Phase volume and interface areas of the discrete phases are also available. This sample was calculated to contain 67% granular material (voxel size and not the Australian texture diagram constrains the range limit), 27% clay/silt defined as material with unresolvable diameter, and 6% porosity, counting only the void phase resolvable. Porosity below resolution is obviously excluded. As a comparison the laser sizing technique supplied figures of 73% sand, 23% silt and 4% clay (the Australian texture diagram). Sieve-hydrometer measurement, although less comprehensive, is an almost universally accepted measure (Fredlund *et al.* 2000). This technique gave values of 74% sand, no silt and 16% clay. The surface area of 2 particular phases is available by summing up all voxel-voxel interfaces for those phases. In this case the surface area of the silt/clay (bulk phase) pore interface was calculated to be 3.7 mm^{-2} . The importance of this parameter becomes apparent when dealing with contaminants that sorb to the clay phase.

PORE SIZE DISTRIBUTION

This parameter is routinely measured empirically (Wang *et al.* 2002) or calculated from the grain size distribution using a PTF (Arya & Paris 1981). Using the image data collected here pore size distribution can be calculated by simulating the mercury porosimetry data or using a function that calculates the maximal sphere size that can fit into any void space defined as void by the segmentation. The maximal sphere size can be seen on the right hand graph in Figure 4. Mean pore size using this measure is $74 \mu\text{m}$.

DISCUSSION

From inspection of the segmented data the clay seems to be pore filling, inhabiting pore space of the same type as the free pore space. This can be seen in the covering sphere radius distribution, which shows almost identical pore silt/clay characteristics, and also comes out from calculations of permeability. This later point and the permeability simulations show there are no large conducting pathways at all. All the parameters calculated from the images generally agree with those calculated by traditional methods. The major advantage of the technique presented here, with respect to the study of unconsolidated porous materials, obviates the need for indirect parameterisation of materials.

REFERENCES

- ARYA L.M. & PARIS J.F. 1981. A physioempirical model to predict the soil moisture characteristic from particle-size distribution and bulk density. *Soil Science Society of America Journal* **45**, 1023-1030.
- BURGER R.L. & BELITZ K. 1997. Measurement of anisotropic hydraulic conductivity in unconsolidated sands: A case study from a shoreface deposit, Oyster, Virginia. *Water Resources Research* **33(6)**, 1515-1522.
- FELDKAMP L.A., DAVIS L.C. & KRESS J.W. 1984. Practical Cone-Beam Algorithm. *Journal of the Optical Society of America A - Optics Image Science and Vision* **1(6)**, 612-619.
- FREDLUND M.D., FREDLUND D.G. & WILSON G.W. 2000. An equation to represent grain-size distribution. *Canadian Geotechnical Journal* **37(4)**, 817-827.
- FREDLUND M.D., WILSON G.W. & FREDLUND D.G. 2002. Use of the grain-size distribution for estimation of the soil-water characteristic curve. *Canadian Geotechnical Journal* **39(5)**, 1103-1117.
- JONES R.M. 2003. Particle size analysis by laser diffraction: ISO 13320, standard operating procedures, and

- Mie theory. *American Laboratory* **35(1)**.
- KNACKSTEDT M.A., ARNS C.H., LIMAYE A., SAKELLARIOU A., SENDEN T.J., SHEPPARD A.R., SOK R.M., PINCZEWSKI W.V. & BUNN G.F. 2004. Digital core laboratory: Reservoir-core properties derived from 3D images. *Journal of Petroleum Technology* **55(5)**, 66-68.
- LIN C.L. & MILLER J.D. 2004. Pore structure analysis of particle beds for fluid transport simulation during filtration. *International Journal of Mineral Processing* **73**, 281-294.
- LOIZEAU L.-L., ARBOUILLE D., SANTIAGO S. & VERNET J.-P. 1994. Evaluation of a wide range laser diffraction grain size analyser for use with sediments. *Sedimentology* **41**, 353-361.
- PARTICLE AND SURFACE SCIENCES PTY. LTD. 2004. Unit 4/31 Dwyer Street, North Gosford, NSW, Australia, 2250. URL: http://www.pss.aus.net/products/micromeritics/equip_particle_size/5200/5200.html.
- MARSHALL T.J. 1947. Mechanical composition of soil in relation to field descriptions of texture. *Council for Scientific and Industrial Research, Australia, Bulletin No.224*.
- AMERICAN SOCIETY FOR TESTING AND MATERIALS 1990. ASTM D 422-63, Standard Test Method for Particle-Size Analysis of Soils. *American Society for Testing and Materials*, 1916 Race Street, Philadelphia, PA 19103.
- PAN C., HILPERT M. & MILLER C.T. 2004. Lattice -Boltzman simulation of two-phase flow in porous media. *Water Resources Research* **40(1)**.
- POWERS M.C. 1953. A new roundness scale for sedimentary particles. *Journal of Sedimentary Petrology* **23**, 117-119.
- RUAN H. & ILLANGASEKARE T.H. 1999. Estimation of relative hydraulic conductivity of sandy soils based on a sheet flow model. *Journal of Hydrology* **219**, 83-93.
- SAHIMI M. 1993. Flow phenomena in rocks: from continuum to fractals, percolation, cellular automata, and simulated annealing. *Reviews of Modern Physics* **65(4)**, 1393-1534.
- SAKELLARIOU A., SAWKINS T.J., SENDEN T.J. & LIMAYE A. 2004. X-ray tomography for mesoscale physics applications. *Physica A* **339**, 152-158.
- SOLYMAR M. & FABRICIUS I.L. 1999. Image Analysis and Estimation of Porosity and Permeability of Arnager Greensand, Upper Cretaceous, Denmark. *Physics and Chemistry of the Earth (A)* **24(7)**, 587-591.
- TURNER M., SAKELLARIOU A., ARNS C., SOK R., LIMAYE A. SENDEN T. & KNACKSTED M. 2003. Towards modelling regolith permeability with high resolution X-ray tomography. In: ROACH I.C. ed. *Advances in Regolith*. CRC LEME, pp. 421-425.
- THE AUSTRALIAN DRILLING INDUSTRY TRAINING COMMITTEE LTD. 1997. *Drilling : The Manual of Methods, Applications, and Management*. CRC Press, Lewis Publishing.
- VOGEL H.-J. & ROTH K. 1998. A new approach for determining effective soil hydraulic functions. *European Journal of Earth Science* **49**, 547-556.
- WANG Q., HORTON R. & LEE J. 2002. A simple model relating soil water characteristic curve and soil solute breakthrough curve. *Soil Science* **167(7)**, 436-443.
- WÖSTEN J.H.M., PACHEPSKY Y.A. & RAWLS W.J. 2001. Pedotransfer functions: bridging the gap between available basic soil data and missing soil hydraulic characteristics. *Journal of Hydrology* **251**, 123-150.